

## RESEARCH ARTICLE

10.1002/2014JD021608

## Key Points:

- The response of terrestrial aridity to global warming in terms of  $P/PET$
- A decrease in  $P/PET$  (i.e., a drier terrestrial climate) by  $\sim 3.4\%/^{\circ}\text{C}$
- Examine the  $P/PET$  change by comparing changes in  $PET$  over land and  $E$  over ocean

## Correspondence to:

Q. Fu,  
qfuatm@gmail.com

## Citation:

Fu, Q., and S. Feng (2014), Responses of terrestrial aridity to global warming, *J. Geophys. Res. Atmos.*, 119, doi:10.1002/2014JD021608.

Received 4 FEB 2014

Accepted 10 JUN 2014

Accepted article online 13 JUN 2014

## Responses of terrestrial aridity to global warming

Qiang Fu<sup>1,2</sup> and Song Feng<sup>3</sup>

<sup>1</sup>College of Atmospheric Sciences, Lanzhou University, Lanzhou, China, <sup>2</sup>Department of Atmospheric Sciences, University of Washington, Seattle, Washington, USA, <sup>3</sup>Department of Geosciences, University of Arkansas, Fayetteville, Arkansas, USA

**Abstract** The dryness of terrestrial climate can be measured by the ratio of annual precipitation ( $P$ ) to potential evapotranspiration ( $PET$ ), where the latter represents the evaporative demand of the atmosphere, which depends on the surface air temperature, relative humidity, wind speed, and available energy. This study examines how the terrestrial mean aridity responds to global warming in terms of  $P/PET$  using the Coupled Model Intercomparison Project phase 5 transient  $\text{CO}_2$  increase to  $2 \times \text{CO}_2$  simulations. We show that the (percentage) increase (rate) in  $P$  averaged over land is  $\sim 1.7\%/^{\circ}\text{C}$  ocean mean surface air temperature increase, while the increase in  $PET$  is  $5.3\%/^{\circ}\text{C}$ , leading to a decrease in  $P/PET$  (i.e., a drier terrestrial climate) by  $\sim 3.4\%/^{\circ}\text{C}$ . Noting a similar rate of percentage increase in  $P$  over land to that in evaporation ( $E$ ) over ocean, we propose a framework for examining the change in  $P/PET$ , in which we compare the change in  $PET$  over land and  $E$  over ocean, both expressed using the Penman–Monteith formula. We show that a drier terrestrial climate is caused by (i) enhanced land warming relative to the ocean, (ii) a decrease in relative humidity over land but an increase over ocean, (iii) part of increase in net downward surface radiation going into the deep ocean, and (iv) different responses of  $PET$  over land and  $E$  over ocean for given changes in atmospheric conditions (largely associated with changes in temperatures). The relative contributions to the change in terrestrial mean aridity from these four factors are about 35%, 35%, 15%, and 15%, respectively. The slight slowdown of the surface wind over both land and ocean has little impact on the terrestrial mean aridity.

## 1. Introduction

The dryness of terrestrial climate can be measured in terms of an aridity index that is defined by the ratio of annual precipitation ( $P$ ) to annual potential evapotranspiration ( $PET$ ) [Middleton and Thomas, 1992]. The  $PET$  is the evaporative demand of the atmosphere, indicating the maximum amount of evaporation one would get, in a given climate, from a well-watered soil vegetation surface [Arya, 2001]. The true evaporation ( $E$ ) over land that usually reflects the amount of water supply (e.g., precipitation) will be less than the  $PET$  unless the soil is saturated with water. The  $P/PET$  ratio is thus a quantitative indicator of the degree of water deficiency at a given location, which may be near zero in desert but can exceed unity in wet climate. Under the United Nations Convention to Combat Desertification [United Nations Convention to Combat Desertification, 1994] classification, drylands are characterized by  $P/PET < 0.65$  and are further divided into hyperarid ( $P/PET < 0.05$ ), arid ( $0.05 < P/PET < 0.2$ ), semiarid ( $0.2 < P/PET < 0.5$ ), and dry subhumid ( $0.5 < P/PET < 0.65$ ) regions [Mortimore, 2009; Hulme, 1996; Middleton and Thomas, 1992]. Knowledge of how anthropogenic climate change will affect the terrestrial aridity is essential for water resource and land use managements, especially over dryland regions [e.g., Mortimore, 2009; Reynolds et al., 2007; Fu, 2008; Fu and Ma, 2008; Overpeck and Udall, 2010].

By analyzing climate model simulations for the period 1948–2100, Feng and Fu [2013] show that the  $P/PET$  decreases in most tropical and midlatitude land regions as the Earth warms. This drying would lead to the world's drylands to become  $5.8 \times 10^6 \text{ km}^2$  (or 10%) larger than the current climatology by the end of this century under a high greenhouse gas emission scenario (Representative Concentration Pathway 8.5 (RCP8.5)). The major expansion of arid regions would occur over southwestern North America, the northern fringe of Africa, southern Africa, and Australia, while major expansions of semiarid regions would occur along the north coast of the Mediterranean, southern Africa, and parts of North and South America [Feng and Fu, 2013]. An increase in aridity and expansion of drylands in response to global warming will increase the fraction of the world's population affected by water scarcity and land degradation. The 21st century drying is also shown by Cook et al. [2014].

Climate models robustly predict an increase in global mean precipitation in response to a CO<sub>2</sub> increase [Mitchell *et al.*, 1987; Allen and Ingram, 2002; Held and Soden, 2006; Lambert and Webb, 2008; Stephens and Ellis, 2008; Pendergrass and Hartmann, 2014]. The projected increase rate is ~1.4% °C<sup>-1</sup>, with respect to global mean surface temperature increase due to a transient CO<sub>2</sub> doubling, and has been attributed to an atmospheric energy budget constraint [e.g., Allen and Ingram, 2002; Pendergrass and Hartmann, 2014]. Here we quantify the change of terrestrial mean *P*/*PET* due to a transient CO<sub>2</sub> increase and discuss the underlying physical processes responsible for it.

Global mean annual precipitation and evaporation must remain equal since the atmosphere is a small reservoir for water. Assuming a similar increase in terrestrial mean precipitation to that over ocean, Sherwood and Fu [2014] argue that the *PET* will increase much faster than *P* in response to global warming, leading to drier conditions over land in the future. This is because land surfaces warm about 50% more rapidly than oceans [e.g., Manabe *et al.*, 1992; Joshi *et al.*, 2008], and relative humidity on average decreases over land but increases over ocean [Simmons *et al.*, 2010; Intergovernmental Panel on Climate Change (IPCC), 2013]. Scheff and Frierson [2014] examined the changes in *PET* fields calculated from the outputs of the global climate models participating in the phase 5 of the Coupled Model Intercomparison Project (CMIP5) [Taylor *et al.*, 2012] between 2081–2099 from the RCP8.5 scenario and 1981–2099 from the historical runs. They showed that the % change in local annual mean *PET* is almost always positive, on average in the low double digits in terms of magnitude, usually increasing with latitude. The increase is dominated by the direct, positive effects of warming at constant relative humidity. However, the rate of percentage change of terrestrial mean *P*/*PET* with respect to temperature increase due to a transient CO<sub>2</sub> increase and its partitioning to changes in relevant meteorological variables has not been quantified and documented before.

This paper examines the change of *P*/*PET* in the 1% increase in CO<sub>2</sub> until the doubled scenario from the CMIP5 global climate models (GCMs). Section 2 describes the methods and data used in this study. The changes in *P* and *E* over both land and ocean and *PET* and *P*/*PET* over land are presented in section 3. The causes of the change in *P*/*PET* are examined in section 4, followed by the summary and conclusions in section 5.

## 2. Methods and Data

### 2.1. The *PET* Algorithm

We calculated the *PET* using the Penman–Monteith algorithm [Maidment, 1993; Allen *et al.*, 1998] that includes the effects of available energy ( $R_n - G$ , where  $R_n$  is the net downward radiation and  $G$  is the heat flux into the ground), surface air temperature ( $T_a$ ), relative humidity (RH), and wind speed ( $u$ ). The Penman–Monteith algorithm was recommended by the Food and Agriculture Organization as the standard method for computing the *PET* [Allen *et al.*, 1998]. This algorithm can be written in the form [Allen *et al.*, 1998; Scheff and Frierson, 2014]

$$PET = \frac{(R_n - G)\Delta(T_a) + \rho_a c_p e^*(T_a)(1 - RH)C_H|u|}{\Delta(T_a) + \gamma(1 + r_s C_H|u|)} / L_v, \quad (1)$$

where  $e^*$  is the saturated water vapor pressure,  $\Delta = de^*/dT$ ,  $\rho_a$  is the surface air density,  $c_p$  is the specific heat of air,  $C_H$  is the bulk transfer coefficient,  $r_s$  is the bulk stomatal resistance under well-watered conditions,  $L_v$  is the latent heat of vaporization for water,  $\gamma = (c_p \rho_s) / (0.622 L_v)$ , where  $p_s$  is the surface pressure, and  $u$  is the wind at 2 m above the surface.

Equation (1) is derived from the standard bulk formulae for the sensible heat (SH) and latent heat (LH) fluxes along with the surface energy budget equation in the forms

$$SH = \rho_a c_p C_H (T_s - T_a) |u|, \quad (2)$$

$$LH = \rho_a L_v C_H (q^*(T_s) - q^*(T_a) RH) |u| / (1 + r_s C_H |u|), \quad (3)$$

$$R_n - G = SH + LH, \quad (4)$$

where  $T_s$  is the temperature at the surface interface,  $LH = PET^* L_v$ , and  $q^*$  is the saturated water vapor mixing ratio (i.e.,  $0.622 e^* / p_s$ ). In equation (3), the water vapor at the surface interface is assumed to be saturated. Equation (3) indicates that *PET* is determined by the vapor pressure deficit, i.e.,  $e^*(T_s) - e^*(T_a) RH$ , and the surface wind.

**Table 1.** A List of CMIP5 GCMs Used in This Study

Model Name	Origin
ACCESS1.0	Commonwealth Scientific and Industrial Research, Australia
ACCESS1.3	Commonwealth Scientific and Industrial Research, Australia
CanESM2	Canadian Centre for Climate, Canada
CCSM4	National Center for Atmospheric Research, USA
CESM1-BGC	National Center for Atmospheric Research, USA
CMCC-CM	Centro Euro-Mediterraneo per i Cambiamenti, Italy
CNRM-CM5	Centre National de Recherches Meteorologiques, France
CNRM-CM5-2	Centre National de Recherches Meteorologiques, France
CSIRO-Mk3.6	Commonwealth Scientific and Industrial Research, Australia
GFDL-CM3	Geophysical Fluid Dynamics Laboratory, USA
GFDL-ESM2G	Geophysical Fluid Dynamics Laboratory, USA
GFDL-ESM2M	Geophysical Fluid Dynamics Laboratory, USA
GISS-E2-H	NASA Goddard Institute for Space Studies, USA
GISS-E2-R	NASA Goddard Institute for Space Studies, USA
HadGEM2-ES	Met Office Hadley Centre, UK
INM-CM4	Institute for Numerical Mathematics, Russia
IPSL-CM5A-LR	Institut Pierre-Simon Laplace, France
IPSL-CM5A-MR	Institut Pierre-Simon Laplace, France
IPSL-CM5B-LR	Institut Pierre-Simon Laplace, France
MIROC5	Atmosphere and Ocean Research Institute, Japan
MIROC-ESM	Japan Agency for Marine-Earth Science and Technology, Japan
MPI-ESM-LR	Max Planck Institute for Meteorology, Germany
MPI-ESM-MR	Max Planck Institute for Meteorology, Germany
MPI-ESM-P	Max Planck Institute for Meteorology, Germany
MRI-CGCM3	Meteorological Research Institute, Japan

The Penman–Monteith algorithm is physically based and is superior to empirically based formulations that usually only consider the effect of temperature [Donohue *et al.*, 2010; Dai, 2011; Sheffield *et al.*, 2012]. In the calculations of PET in this paper, we used a  $r_s$  of 70 s/m and a  $C_H$  of  $4.8 \times 10^{-3}$  [Allen *et al.*, 1998]. Scheff and Frierson [2014] used equation (1) with similar  $r_s$  and  $C_H$  values.

The actual evaporation ( $E$ ) over ocean can be considered as the potential evaporation over water. Since equations (2)–(4) are valid over water by setting  $r_s = 0$ , we used equation (1) to calculate the actual evaporation ( $E$ ) over ocean with  $r_s = 0$ . Additionally, we used a  $C_H$  of  $1.5 \times 10^{-3}$  over ocean [Richter and Xie, 2008; I. Richter, personal communication, 2014]. We will compare the  $E$  and its change over ocean as obtained from the Penman–Monteith algorithm with their counterparts obtained directly from the models. As we will discuss later, this is a very useful approach that permits us to place PET over land and  $E$  over ocean in the same framework as a basis for interpreting the changes of terrestrial mean aridity in response to global warming.

In the calculation of PET over land ( $E$  over ocean) using equation (1), we used the actual LH + SH to replace  $R_n - G$  [Scheff and Frierson, 2014]. Although the actual LH and SH over land for the given  $R_n - G$  are different from those derived from equations (2)–(4), where a saturated water vapor is assumed at the surface, their summations are the same following equation (4). Finally, the change in the surface stability (i.e.,  $T_a - T_s$ ) over ocean can be derived in the Penman–Monteith framework, which will also be compared with that obtained directly from the CMIP5 models.

## 2.2. CMIP5 Data

We used the output from the 25 global climate models (Table 1) that participated in the CMIP5 transient CO<sub>2</sub> 1%/yr increase (1pctCO<sub>2</sub>) experiments [Taylor *et al.*, 2012]. The 1pctCO<sub>2</sub> experiment is designed to diagnose transient climate response to 1% yr<sup>-1</sup> CO<sub>2</sub> increase, which is initialized from the multicentury preindustrial quasi-equilibrium control simulations. The models were integrated for 140 years, but only the first 70 years of the data were analyzed in our study. For models with multiple-ensemble simulations, the first ensemble run was used. The change was taken as the difference between the averages for the years 61–70 and 1–10 of the simulations, where the year 70 corresponds to the time of

**Table 2.** Annual Mean Values in the First 10 Years of the Transient CO<sub>2</sub> Increase Simulations (1pctCO<sub>2</sub>) Averaged Over Land, Ocean, and Globe From the Ensemble Average of 25 CMIP5 GCMs (The Numbers in the Parentheses Indicate 1 Standard Deviation of the 25 Model Results)<sup>a</sup>

	Land	Ocean	Globe	Globe (obs)
$P$ (mm)	870 (90)	1194 (55)	1083 (55)	1124 (128)
$E$ (mm)	604 (60)	1300 (62)	1083 (55)	1124 (128)
PET (mm)	1112 (66)	not applicable (NA)	NA	NA
$T_a$ (°C)	12.2 (1.0)	15.7 (0.6)	13.5 (0.6)	13.8
RH (%)	66.8 (3.3)	81.0 (3.7)	77.3 (3.0)	77.7
$u$ (m/s)	3.1 (0.5)	7.1 (0.5)	6.0 (0.5)	3.8
$R_n - G$ (W/m <sup>2</sup> )	85.4 (5.3)	118.1 (4.5)	106.0 (4.0)	112 (12)
$R_n$ (W/m <sup>2</sup> )	86.2 (5.4)	119.0 (3.9)	106.8 (3.6)	112.6 (12)
$R_{n,s}$ (W/m <sup>2</sup> )	159.0 (7.3)	174.9 (4.3)	167.1 (3.5)	165 (7)
$R_{n,L}$ (W/m <sup>2</sup> )	-72.7 (6.6)	-55.9 (3.7)	-60.3 (3.8)	-52.4 (10)

<sup>a</sup>The quantities include precipitation ( $P$ ), evaporation ( $E$ ), potential evapotranspiration (PET), near-surface air temperature ( $T_a$ ), relative humidity (RH), surface wind speed ( $u$ ), available energy ( $R_n - G$ ), net downward radiation ( $R_n$ ), net downward solar radiation ( $R_{n,s}$ ), and net downward long-wave radiation ( $R_{n,L}$ ). Observed global mean quantities are also shown for the comparison:  $T_a$ , RH, and  $u$  are from National Centers for Environmental Prediction reanalysis during 1961–1990, and others are from Stephens *et al.* [2012], with the observational uncertainties in the parentheses.

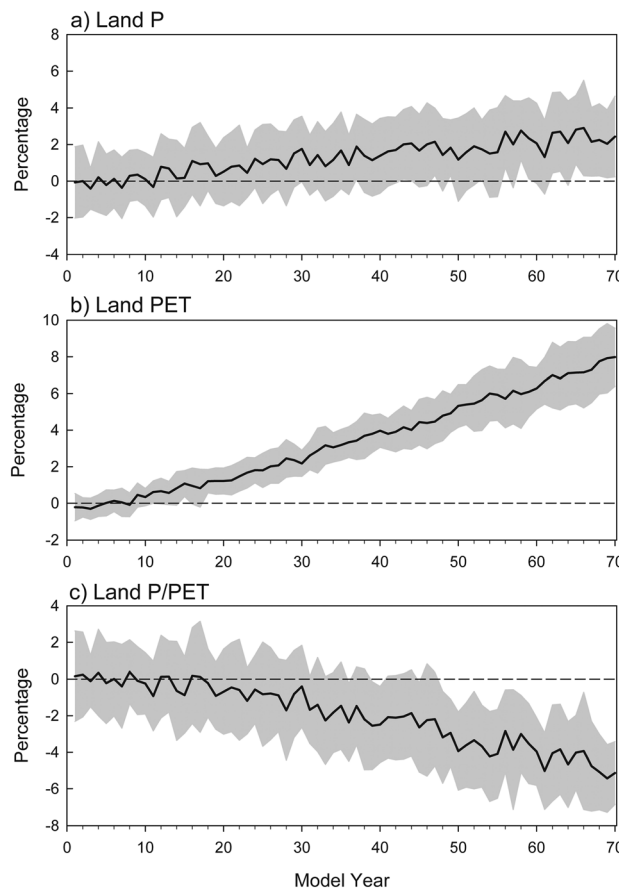


**Figure 1.** Temporal variations of annual mean (a) precipitation ( $P$ ), (b) potential evapotranspiration (PET), and (c) aridity index ( $P/PET$ ) averaged over land (The aridity index shown here is the annual mean  $P$  averaged over land divided by annual mean PET averaged over land). The black lines are the ensemble average of the 25 CMIP5 1pctCO<sub>2</sub> simulations, and the grey shading denotes 1 standard deviation of the 25 models. The units are in percentage anomalies relative to the averaged values of the first 10 years.

CO<sub>2</sub> doubling. Note that only the change in the CO<sub>2</sub> is considered in the 1pctCO<sub>2</sub> experiment, while the RCP scenario experiment considered the changes in land use, aerosols, CO<sub>2</sub>, as well as other greenhouse gases.

In this study, we define the land as the terrestrial regions between 60°S and 90°N, which covers 26.5% of the globe. We will present results averaged over land, ocean, and over the globe. The ocean covers 70.8% of the globe, and the remaining 2.7% of the globe is Antarctica.

The ensemble mean of the 25 models used in this study should be interpreted as our best estimate of climate response to the CO<sub>2</sub> increase. In contrast, the individual ensemble members simulate random internal variations of the climate system, and they contain biases inherent in individual models. Here we use 1 standard deviation of the 25 models as a measure of uncertainties associated with natural variations and model errors.

Table 2 shows the annual mean values of the first 10 years for  $P$ ,  $E$ , PET,  $T_a$ , RH,  $u$ ,  $R_n - G$ ,  $R_n$ ,  $R_{n,s}$ , and  $R_{n,L}$ , averaged over land, ocean, and the globe from the ensemble mean of the 25 CMIP5 models. The numbers in the parentheses indicate the 1 standard deviation of the 25 model results. As expected, the global

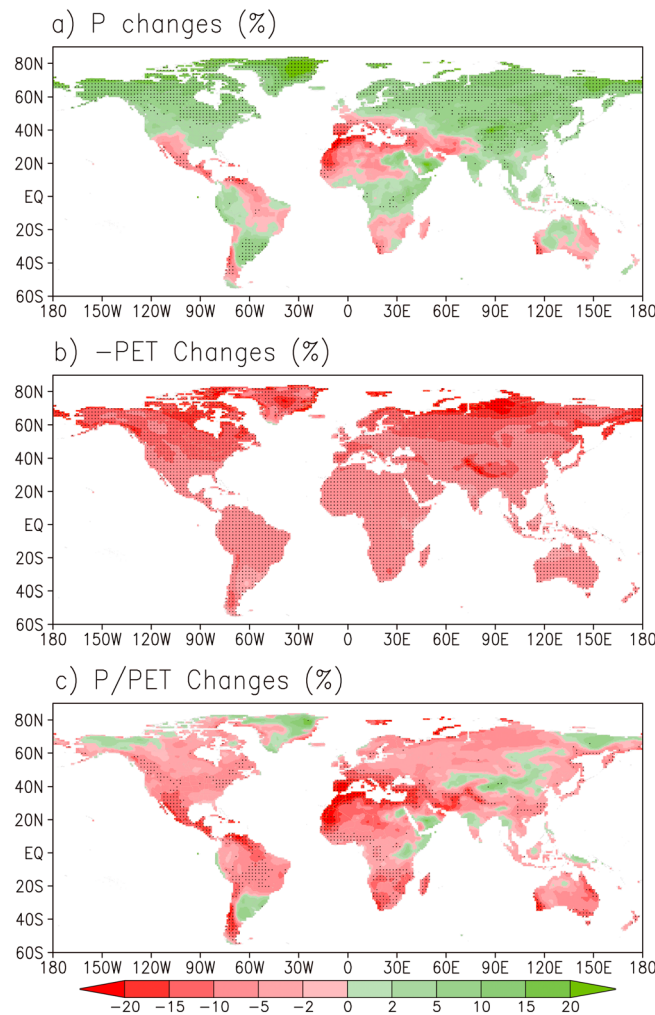


**Figure 2.** Global distributions of percentage changes (%) in (a)  $P$ , (b)  $-PET$ , and (c)  $P/PET$  taken as the difference between the averages for the years 61–70 and 1–10 of the CMIP5 1pctCO<sub>2</sub> simulations ( $P/PET$  is calculated as the averaged  $P$  divided by averaged  $PET$ ). Grid points are stippled when more than 80% of the 25 models agree on the sign.

mean precipitation and evaporation are the same and are equivalent to a latent heat flux (i.e.,  $L_v P$ ) of  $84.8 \text{ Wm}^{-2}$ . Note that the global mean precipitation (latent heat flux),  $R_n - G$ , sensible heat flux (i.e.,  $R_n - G - LH$ ), and net downward radiation, as well as its short-wave and long-wave components, agree well with the observations within observational uncertainties (Table 2). The simulated  $T_a$  and RH values agree well with those from the reanalysis, while the simulated global mean surface wind speed is larger than that from the reanalysis.

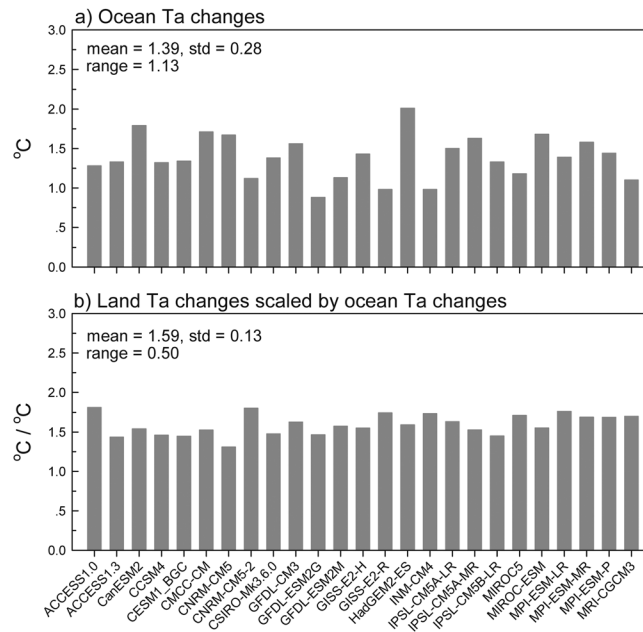
The percentage changes in various surface variables (e.g., mean precipitation over land) from each model are scaled by the change in surface air temperature averaged over ocean, which defines the rate of percentage change. We use the ocean mean surface air temperature increase rather than the global mean temperature increase for scaling because the change in land surface air temperature is largely determined by that over ocean [e.g., Manabe et al., 1992; Joshi et al., 2008]. The use of the ocean mean surface air temperature change for scaling also helps facilitate the interpretation of the  $P/PET$  changes in terms of the evaporation over ocean.

### 3. Changes of $P$ , $E$ , $PET$ , and $P/PET$

#### 3.1. Temporal Variations in $P$ , $PET$ , and $P/PET$ and Spatial Patterns of the Changes

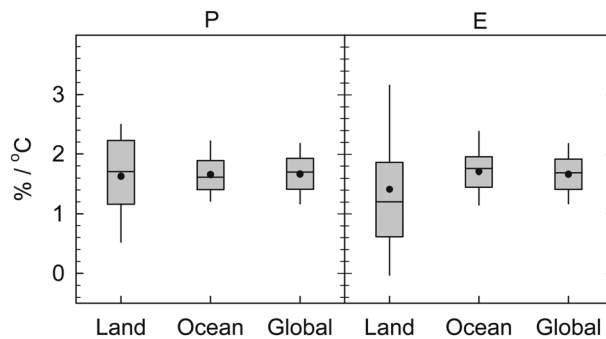
Figure 1 shows the time series of annual mean  $P$ ,  $PET$ , and  $P/PET$ , averaged over land, in units of percentage anomalies with respect to averaged values of the first 10 years. We see increases in  $P$  and  $PET$  but a decrease in  $P/PET$  due to an increase in CO<sub>2</sub> concentration in the atmosphere. An increase in  $P$  cannot keep pace with the increasing  $PET$ , causing a decrease in  $P/PET$  (Figure 1).

Figure 2 shows the global distributions of the percentage changes in  $P$ ,  $-PET$ , and  $P/PET$  between the years 61–70 and 1–10. Note that the summation of percentage changes in  $P$  and  $-PET$  is approximately equal to the percentage change in  $P/PET$  (see equation (5)). The spatial patterns shown in Figure 2 are very similar to those of the changes in  $P$ ,  $PET$ , and  $P/PET$  at the end of the 21st century relative to current climate, from the CMIP5 scenario RCP8.5 simulations [see Feng and Fu, 2013, Figures 7 and 8]. One important difference is that the area of precipitation decrease near the Mediterranean Sea, associated with the CO<sub>2</sub> increase only (Figure 2a), is significantly larger (extending more east and south) as compared with that due to changes in not only CO<sub>2</sub> but also aerosols, land surface, ozone, and other greenhouse gases in RCP8.5. This leads to a larger drying area over northern Africa and Asia (Figure 2c).



**Figure 3.** (a) The change of surface air temperature ( $T_a$ ) averaged over ocean, taken as the difference between the averages for the years 61–70 and 1–10 of the CMIP5 1pctCO<sub>2</sub> simulations, versus individual models. (b) The change of surface air temperature ( $T_a$ ) averaged over land scaled by ocean mean surface air temperature change. The multimodel ensemble mean value along with its standard deviation and range is shown in each panel.

intermodel differences are significantly larger for land  $P$  changes, which reflects a larger interannual variability in  $P$  over land (not shown). Alternatively, the global mean  $P$  change scaled by the ocean  $T_a$  change (i.e., 1.66%/°C) can be rescaled as the global mean  $P$  change divided by the global mean  $T_a$  change: 1.66%/°C/1.16 = 1.43%/°C, which is consistent with previous studies [e.g., Pendergrass and Hartmann, 2014]. As for  $P$ , land  $E$  changes show larger intermodel differences than ocean  $E$ . The multimodel mean value for land  $E$  changes is smaller than that for ocean  $E$ . Figure 4 shows that the rate of percentage change of



**Figure 4.** Percentage (%) changes in (left) annual mean  $P$  and (right) evaporation ( $E$ ) averaged over land, ocean, and globe, scaled by ocean mean surface air temperature increases (°C) from the CMIP5 1pctCO<sub>2</sub> simulations. The results are plotted with box and whisker diagrams representing percentiles of changes computed from the 25 models. The central line (black dot) within each box represents the median (mean) value of the model ensemble. The top and bottom of each box shows the 75th and 25th percentiles, and the top and bottom of each whisker display the 95th and 5th percentile values in the ensemble, respectively.

**3.2. Rates of Change in  $P$ ,  $E$ , PET, and  $P/PET$**

Before presenting the rates of change in  $P$ ,  $E$ , PET, and  $P/PET$ , Figure 3 shows the ocean  $T_a$  changes (Figure 3a) and the ratio of  $T_a$  changes over land and ocean (Figure 3b) from the individual models. The ensemble mean ocean  $T_a$  increases by 1.39°C, with a standard deviation of 0.28°C, while the mean land to ocean ratio is 1.59, with a standard deviation of 0.13. The global mean  $T_a$  increase per °C ocean  $T_a$  increase is 1.16 with a standard deviation of 0.03 (not shown).

Figure 4 shows the percentage change rates in annual mean precipitation (left) and evaporation (right) averaged over land, ocean, and the globe. The multimodel ensemble mean precipitation change rates over land and ocean are both ~1.65%/°C, supporting the statement of Sherwood and Fu [2014] that the mean precipitation over land and ocean changes similarly. Note that the

ocean  $E$  is very similar to those of both land and ocean  $P$ , indicating that the averaged  $P$  changes over both land and ocean are largely constrained by the evaporation over ocean.

Figure 5 shows the rates of percentage change in annual mean PET (middle) and  $P/PET$  (right) over land. The change rate in  $P$  is also shown in Figure 5 (left) for a direct comparison. The multimodel ensemble mean rate is 5.3%/°C for PET, which is much larger than the rate of increase of precipitation. All models project a drier future climate over land [Feng and Fu, 2013; Cook et al., 2014]. The multimodel mean change rate in the aridity index is -3.4%/°C. Figure 5 indicates that although land on average will get more precipitation in a warming climate, it will not get enough to keep pace with the growing evaporative demand, leading to a drier

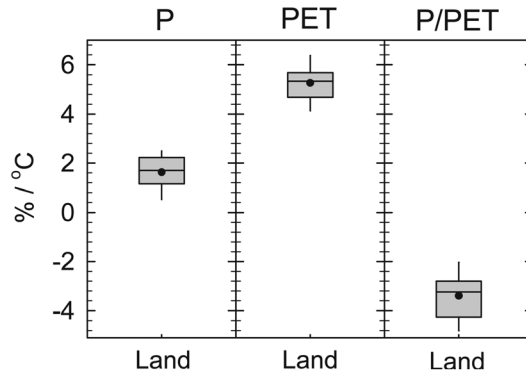


**Figure 5.** Percentage (%) changes in the (left) annual mean  $P$ , (middle)  $PET$ , and (right)  $P/PET$  averaged over land, scaled by ocean mean surface air temperature increases ( $^{\circ}C$ ) from the CMIP5 1pctCO<sub>2</sub> simulations. The results are plotted with box and whisker diagrams as defined in Figure 4.

terrestrial climate [Sherwood and Fu, 2014]. Below, we will examine the effects of changes in various surface meteorological variables including surface air temperature, relative humidity, wind speed, and available energy on the  $P/PET$  changes.

#### 4. Attributions of $P/PET$ Changes Over Land

The percentage change in  $P/PET$  can be written in the following form [Feng and Fu, 2013]:

$$\Delta\left(\frac{P}{PET}\right) / \left(\frac{P}{PET}\right) \approx \frac{\Delta P}{P} - \frac{\Delta PET}{PET}. \quad (5)$$

Approximating the percentage change in  $P$  over land with  $E$  over ocean, equation (5) becomes

$$\Delta\left(\frac{P}{PET}\right) / \left(\frac{P}{PET}\right) \approx \left(\frac{\Delta E}{E}\right)_{\text{Ocean}} - \frac{\Delta PET}{PET}. \quad (6)$$

Since the actual evaporation over ocean is the same as the potential evaporation there, which can also be derived using the Penman–Monteith algorithm, we can examine the change in  $P/PET$  in the framework of the  $PET$  by comparing its changes over land and ocean (see equation (6)). Table 3 shows that the  $E$  and its change over ocean from the Penman–Monteith algorithm are consistent with those obtained directly from the GCMs.

Sherwood and Fu [2014] argue that the differences between  $\frac{\Delta PET}{PET}$  and  $\left(\frac{\Delta E}{E}\right)_{\text{Ocean}}$  are largely caused by the enhanced warming over land relative to ocean as well as the relative humidity changes over land and ocean with opposite sign. Here we quantify these effects as well as the effects of changes in wind speed and available energy at the surface. Before doing so, we first present the changes in relevant surface meteorological variables over land and those over ocean.

##### 4.1. Changes in $T_a$ , $RH$ , $u$ , and $R_n - G$ Over Land and Ocean

The rates of change in  $T_a$ ,  $RH$ ,  $u$ , and  $R_n - G$  over land and ocean are shown in Figure 6. The rate of change in surface air temperature over ocean is one following the definition.

The GCMs suggest that  $T_a$  over land increases ~60% faster than  $T_a$  over ocean with small model-to-model differences (Figure 6, left). This phenomenon is well documented and discussed in literatures [e.g., Manabe et al., 1992; Joshi et al., 2008; Byrne and O’Gorman, 2013]. A larger warming would lead to a larger  $PET$  increase [Feng and Fu, 2013; Scheff and Frierson, 2014]. Therefore, there is a larger increase in  $PET$  over land than the increase in  $E$  over ocean due to the direct temperature effects.

The  $RH$  over land decreases in almost all the GCMs with a mean value of  $-0.76\%/^{\circ}C$ , while it increases in all the GCMs over ocean with a mean value of  $0.27\%/^{\circ}C$  (Figure 6, middle left). Previous studies also show a decrease in  $RH$  over land and an increase over ocean from both model simulations and observations [Rowell and Jones, 2006; Richter and Xie, 2008; Simmons et al., 2010; O’Gorman and Muller, 2010]. Since  $PET$

**Table 3.** Comparison of Annual Mean Evaporation ( $E$ ) and Its Percentage Change Rate and Surface Stability ( $T_a - T_s$ ) Change Rate Over Ocean Estimated Using the Penman–Monteith Algorithm and Those Directly From the GCMs<sup>a</sup>

	$E$ (mm)	Percentage Change Rate in $E$ ( $\%/^{\circ}C$ )	Change Rate in $T_a - T_s$ ( $^{\circ}C/^{\circ}C$ )
Penman–Monteith	1267 (90)	1.92 (0.39)	0.07 (0.03)
Directly from the GCMs	1300 (62)	1.71 (0.40)	0.06 (0.02)

<sup>a</sup>The ensemble mean values along with 1 standard deviation (the numbers in the parentheses) of the 25 model results are shown.

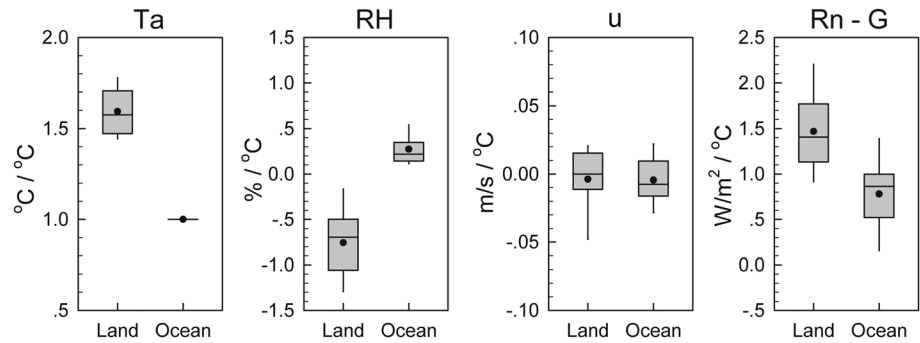


**Figure 6.** Changes in (left)  $T_a$ , (middle left) relative humidity (RH), (middle right) wind speed ( $u$ ), and (right) available energy ( $R_n - G$ ) averaged over land and ocean, scaled by ocean mean surface air temperature increases, from the CMIP5 1pctCO<sub>2</sub> simulations. The results are plotted with box and whisker diagrams as defined in Figure 4.

increases with decreasing RH (see equation (1)), the changes in RH over land (ocean) would result in an increase (a decrease) of PET ( $E$ ) over land (ocean), leading to a larger difference between land PET and ocean  $E$ . Note that the multimodel mean value of the global mean RH changes is near 0 (not shown).

The mean rates of change of surface wind speeds over land and ocean are both  $-0.004$  m/s/°C (Figure 7, middle right). Therefore, they should have little effect on the changes of PET over land and  $E$  over ocean. The changes of PET over land and  $E$  over ocean are then largely caused by the changes in the vapor pressure deficit that are thus about  $5.3\%/^{\circ}\text{C}$  over land and  $1.7\%/^{\circ}\text{C}$  over ocean. It is interesting to notice that there is a significant decrease in observed surface wind speeds globally [McVicar et al., 2012]. For example, about 40% decrease in surface wind was reported in the last 4 decades over India [Padmakumari et al., 2013]. Aerosols could cause the decrease of surface wind [Yang et al., 2013]. Understanding of observed changes in surface wind and its impact on the PET ( $E$ ) are beyond the scope of the present study but will be addressed in our future research effort.

PET is proportional to the available energy ( $R_n - G$ ). The rates of change of  $R_n - G$  over land and ocean are shown in Figure 6 (right). The multimodel mean value is  $1.47$  W/m<sup>2</sup>/°C over land and  $0.78$  W/m<sup>2</sup>/°C over ocean. Therefore, the change in  $R_n - G$  may also contribute to a larger increase in PET over land than  $E$  over ocean. By comparing the net downward radiation changes in Figure 7 (left) with the  $R_n - G$  changes in Figure 6 (right), we note that there is a near-zero  $G$  change over land but a rate of change of  $\sim 1.0$  W/m<sup>2</sup>/°C over ocean. Despite the slightly smaller  $R_n$  increase over land than over ocean (Figure 7, left), there is a larger increase in  $R_n - G$  over land, because part of the increased net downward radiation at the ocean surface is

transported to deep ocean [Hansen et al., 2005; Johnson et al., 2011; Loeb et al., 2012; Stephens et al., 2012].

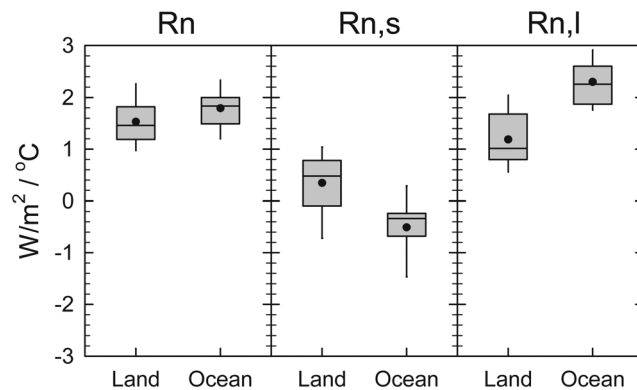


**Figure 7.** Changes in (left) net downward radiation ( $R_n$ ), (middle) net downward short-wave radiation ( $R_{n,s}$ ), and (right) net downward long-wave radiation ( $R_{n,l}$ ) averaged over land and ocean, scaled by ocean mean surface air temperature increases, from the CMIP5 1pctCO<sub>2</sub> simulations. The results are plotted with box and whisker diagrams as defined in Figure 4.

It is also interesting to note that there is an increase in  $R_{n,s}$  over land but a decrease over ocean, although both are statistically insignificant (Figure 7, middle). There is a significant increase in  $R_{n,l}$  over both land and ocean, and the increase over land is smaller (Figure 7, right). The atmospheric warming due to CO<sub>2</sub> leads to more H<sub>2</sub>O in the atmosphere. The increase of both CO<sub>2</sub> and H<sub>2</sub>O causes larger downward surface infrared radiation. A smaller  $R_{n,l}$  but a larger  $R_{n,s}$  over land than those over ocean indicate a decrease in cloud fraction over land relative to that over ocean.

**Table 4.** Effects of Surface Air Temperature ( $T_a$ ), Relative Humidity (RH), Wind Speed ( $u$ ), and Available Energy ( $R_n - G$ ) on the Percentage Change Rates in Potential Evapotranspiration (PET) Over Land, Evaporation ( $E$ ) Over Ocean, and  $P/PET$  Over Land, Estimated Using the Penman–Monteith Algorithm Based on 25 CMIP5 1pctCO<sub>2</sub> Increase to 2 × CO<sub>2</sub> Simulations<sup>a</sup>

	PET (%/°C)	$E$ (%/°C)	$P/PET$ (%/°C)	Relative Contribution to the Total $P/PET$ Change (%)
$T_a$	3.48	1.68 (2.19, -0.51)	-1.80 (-1.29, -0.51)	53 (38, 15)
RH	0.95	-0.31 (-0.34, 0.03)	-1.26 (-1.29, 0.03)	37 (38, -1)
$u$	-0.03	-0.06 (-0.03, -0.03)	-0.03 (0.0, -0.03)	1 (0, 1)
$R_n - G$	0.88	0.62 (0.47, 0.15)	-0.26 (-0.41, 0.15)	8 (12, -4)
Total	5.28	1.92 (2.29, -0.37)	-3.36 (-2.99, -0.37)	100 (89, 11)

<sup>a</sup>The percentage change in  $P/PET$  is approximated by equation (6). The first number in parentheses gives the change based on the Penman–Monteith algorithm using the land coefficients and background atmospheric conditions, while the second one is the effect of differences in coefficients and background conditions between land and ocean. See the text and Appendix A for the details on the methods.

The evaporation change over ocean corresponds to a change of  $1.73 \text{ Wm}^{-2}/^\circ\text{C}$  in terms of latent heat flux. Noting the change of  $0.78 \text{ Wm}^{-2}/^\circ\text{C}$  in  $R_n - G$  or  $\text{SH} + \text{LH}$ , we have a change of  $-0.95 \text{ Wm}^{-2}/^\circ\text{C}$  in  $\text{SH}$  over ocean. Using equation (2), we obtain a rate of change of  $0.07^\circ\text{C}/^\circ\text{C}$  for  $T_a - T_s$ , which is consistent with that obtained directly from the GCMs (Table 3). Richter and Xie [2008] show that ocean surface evaporation increases by  $2\%/^\circ\text{C}$  of surface warming, rather than the  $7\%/^\circ\text{C}$  rate simulated for atmospheric moisture, because of the increase in surface relative humidity and surface stability and the decrease in surface wind speed. In the framework of the Penman–Monteith algorithm, the change in  $T_a - T_s$  along with  $E$ , scaled by the  $T_a$  change, is predicted by the changes in available energy, surface wind, and relative humidity.

#### 4.2. Effects of Changes in $T_a$ , RH, $u$ , and $R_n - G$ Upon $P/PET$

Using equation (1) to calculate the evaporation over ocean, we obtain a rate of percentage change of  $\sim 1.9\%/^\circ\text{C}$  in the annual mean evaporation over ocean (Table 3), similar to that obtained directly from models. Here we employ equation (1) to quantify the individual contributions of changes in temperatures, relative humidity, wind speed, and available energy to the total percentage changes in PET over land,  $E$  over ocean, and ultimately  $P/PET$  over land. For example, in order to isolate the effect of the temperature change on PET over land, we calculate the PET using  $T$  in the last 10 years but RH,  $u$ , and  $\text{SH} + \text{LH}$  from the first 10 years and compare it with PET using the inputs from the first 10 years. See Appendix A for the details on the method of deriving the individual contributions.

The second (third) column of Table 4 shows that the change in PET ( $E$ ) over land (ocean) is dominated by the change in temperatures, while the changes in RH and available energy also make appreciable contributions [Scheff and Frierson, 2014]. (The numbers in the parentheses will be discussed later.) The increase in temperatures results in a larger PET over land and a larger  $E$  over ocean (see second row in Table 4), but the former is more than twice as large as the latter. This is because of the enhanced warming (60%) over land relative to that over ocean and also partly because the  $E$  over ocean is less sensitive to temperature when  $r_s = 0.0$  [Scheff and Frierson, 2014].

The decrease (increase) in RH over land (ocean) results in an increase (decrease) in PET ( $E$ ) (see the third row in Table 4) and hence a larger difference between PET and  $E$ . The increase in available energy over both land and ocean increases PET over land and  $E$  over ocean (see the fifth row in Table 4). However, the increase in available energy over ocean, and thus  $E$ , is smaller because part of downward radiation is transported downward into the deep ocean (section 4.1). Surface wind speed changes little and thus makes little contribution to the change of terrestrial mean aridity (see the fourth row in Table 4).

The net contributions from individual surface meteorological variables (i.e.,  $T_a$ , RH,  $u$ , and  $R_n - G$ ) to the changes in  $P/PET$  are the differences between the third and second columns following equation (6), which are shown in the fourth column in Table 4. In terms of the total change rate in  $P/PET$ , they correspond to relative contributions of 53%, 37%, 1%, and 8%, respectively (see the fifth column in Table 4). Note that these contributions are not only determined by the contrasting changes over land and ocean in surface meteorological variables but also are affected by the coefficients and background atmospheric

**Table 5.** Same as Table 4 Except That the First Number in the Parentheses Gives the Change Based on the Penman–Monteith Algorithm Using the Ocean Coefficients and Background Atmospheric Conditions, While the Second One is the Effect of Differences in Coefficients and Background Conditions Between Ocean and Land

	PET (%/°C)	E (%/°C)	P/PET (%/°C)	Relative Contribution to the Total P/PET Change (%)
$T_a$	3.48 (2.67, 0.81)	1.68	-1.80 (-0.99, -0.81)	53 (30, 23)
RH	0.95 (0.87, 0.08)	-0.31	-1.26 (-1.18, -0.08)	37 (35, 2)
$u$	-0.03 (-0.06, 0.03)	-0.06	-0.03 (0.0, -0.03)	1 (0, 1)
$R_n - G$	0.88 (1.17, -0.29)	0.62	-0.26 (-0.55, 0.29)	8 (16, -8)
Total	5.28 (4.65, 0.63)	1.92	-3.36 (-2.73, -0.63)	100 (81, 18)

conditions used in the Penman–Monteith equation, which affect the sensitivity of PET ( $E$ ) to the changes in these variables.

The first number in the parenthesis of the third column in Table 4 is the second column scaled by  $\Delta x_O/\Delta x_L$ , where  $\Delta x_O$  and  $\Delta x_L$  are the changes in the corresponding surface variables from the multimodel ensemble means over ocean and land, respectively. We have  $\Delta x_O/\Delta x_L = 0.628, -0.355, 1.0$ , and  $0.531$  for changes in  $T_a$ , RH,  $u$ , and SH + LH, respectively. For example, we have  $3.48 \times 0.628 = 2.19$ . They thus can be considered as the  $E$  changes over ocean from the Penman–Monteith algorithm using the land coefficients ( $r_s$  and  $C_H$ ) and the background atmospheric conditions. The second number in the parentheses is the difference between the number outside the parentheses and the first number inside them. It shows the effect of using the coefficients and background atmospheric conditions over ocean versus those over land for given changes in atmospheric conditions. The numbers in the parentheses in the fourth and fifth columns are the corresponding values for the changes in P/PET and the relative contributions, respectively. These numbers thus show the effects of contrasting changes in surface meteorological variables over land and ocean, versus those due to the use of the different (land versus ocean) coefficients and background atmospheric conditions in estimating the effects of given atmospheric changes. Therefore, the causes of the drier terrestrial climate are further quantified here in terms of (i) enhanced land warming relative to ocean, (ii) a decrease in RH over land but an increase over ocean, (iii) part of increase in net downward radiation going into the deep ocean, and (iv) different responses of PET over land and  $E$  over ocean for given changes in atmospheric conditions. The relative contributions to the change in terrestrial mean aridity from these four factors are 38%, 38%, 12%, and 11%, respectively (Table 4).

**Table 6.** Relative Contributions of Surface air Temperature ( $T_a$ ), Relative Humidity (RH), Wind Speed ( $u$ ), and Available Energy ( $R_n - G$ ) on the Percentage Change Rates in P/PET<sup>a</sup>

	Relative Contribution to the Total P/PET Change (%)
$T_a$	53 (34 ± 4, 19 ± 4)
RH	37 (36 ± 2, 0 ± 2)
$u$	1 (0 ± 0, 1 ± 0)
$R_n - G$	8 (14 ± 2, -6 ± 2)
Total	100 (85 ± 4, 15 ± 4)

<sup>a</sup>The first number in the parentheses gives the relative contributions of contrasting changes of  $T_a$ , RH,  $u$ , and  $R_n - G$  based on the Penman–Monteith algorithm using the same coefficients and background atmospheric conditions over land and ocean. The second number in the parentheses is the corresponding contributions due to differing responses of PET over land and  $E$  over ocean to given changes in atmospheric conditions. The uncertainties are associated with reference coefficients and background conditions that are used either over ocean or land.

Table 4 (and Tables 5 and 6 later) confirms that the PET over land is more sensitive to the surface air temperature than the  $E$  over ocean. This is because the denominator in equation (1) becomes more sensitive to temperature when  $r_s = 0.0$  over ocean, canceling larger part of the temperature sensitivity of the numerator. It also indicates that the  $E$  over ocean is more sensitive to the available energy change. This is because the energy term in equation (1) makes up a larger proportion of the numerator due to a smaller  $C_H$  over ocean. The PET over land and  $E$  over ocean however respond similarly to a given change in RH (Table 4). Overall, the effect of differing responses of PET over land versus  $E$  over ocean for given changes in atmospheric conditions is largely associated with changes in temperatures.

Table 5 is the same as Table 4 except that the first number in the parentheses gives the change based on the Penman–Monteith algorithm using the ocean coefficients and background atmospheric conditions, while the second one is the effect of the differences in coefficients and background conditions between land and ocean for given atmospheric condition changes over land. The relative contributions (the numbers in the parentheses of the fifth

column) using the ocean coefficients and atmospheric background conditions (Table 5) are slightly different from those using the land conditions (Table 4). By taking the average of the fifth columns from Tables 4 and 5, we obtain the Table 6. It shows that the relative contributions to the change in terrestrial mean aridity are about 35%, 35%, 15%, and 15%, respectively, due to contrasting changes over land versus ocean in  $T_a$ , RH, SH + LH, and differing responses of PET over land and  $E$  over ocean to given changes in atmospheric conditions.

In this study, we used a  $C_H$  of  $4.8 \times 10^{-3}$  and a  $r_s$  of 70 s/m, corresponding to a grass-like surface [Allen *et al.*, 1998], as universal constants over land. Scheff and Frierson [2014] examined the effect of setting  $r_s = 0$ , as used by Burke *et al.* [2006] and Dai [2013], as well as in the case of pan evaporation. It is found that the change in PET due to  $T_a$  becomes 24% smaller. Since such effect on the PET changes associated with other meteorological variables is negligible, the percentage change rate in PET is about 4.6%/°C from 5.3%/°C  $\times$  (0.53  $\times$  0.76 + 0.37 + 0.01 + 0.08) (see Table 4), and the percentage change rate in  $P$ /PET becomes about  $-2.9\%/^{\circ}\text{C}$ , when  $r_s = 0$ . Scheff and Frierson [2014] also examined a “rough,” forest-like surface, and they found a slightly stronger PET response to  $T_a$  than the “smooth” grass surface. Therefore, the results presented in this study are robust and are not very sensitive to the widely different choices of vegetation parameters used in the Penman–Monteith algorithm.

The observed pan evaporation has not increased as expected over the past few decades [Wang *et al.*, 2012]. This is because significant global “stilling” of near-surface winds and slight decreases in downward surface solar radiation compensate for or even exceed the changes due to temperature and relative humidity [McVicar *et al.*, 2012]. But neither the stilling of winds nor the reduced surface insolation appears to be connected to global temperature rise, and the suggested causes are instead associated with land use, aerosols, and/or internal variability [Bichet *et al.*, 2012; Wever, 2012; Yang *et al.*, 2013; McVicar *et al.*, 2012]. Recently, Zhang and Cai [2013] showed that projected crop water deficits at the end of the 21st century are likely to decline slightly despite the rising temperature. They used an empirical equation for PET as a function of the temperature and diurnal temperature range (DTR), developed by Hargreaves and Samani [1985], where the effect of solar radiation is parameterized in terms of DTR. In a warming climate caused by the increase of greenhouse gases, the DTR will decrease [IPCC, 2013], while the  $R_{n,s}$  will increase (see Figure 7, middle). The bottom line is that the decrease in PET caused by the decrease in DTR from the empirical equation has no physical basis for the long-term climate change. In addition, the empirical equation does not consider the effect of changes in RH and  $R_{n,l}$ , both contributing to the increase in PET. It is important to notice here that an empirical relationship may not be appropriate being applied to the long-term climate change at all, although it may fit the current climate reasonably well.

## 5. Summary and Conclusions

The dryness of terrestrial climate can be expressed in terms of the ratio of annual precipitation ( $P$ ) to potential evapotranspiration (PET). The PET is the evaporative demand of the atmosphere, indicating the maximum amount of evaporation one would get, in a given climate, from a well-watered surface. PET is a function of surface air temperature, relative humidity, wind speed, and available energy. This study examines how the terrestrial mean aridity responds to global warming in terms of  $P$ /PET using the CMIP5 transient  $\text{CO}_2$  1%/yr increase to  $2 \times \text{CO}_2$  simulations. We calculated the PET using the Penman–Monteith algorithm, which is based on the bulk formulae for the sensible heat and latent heat fluxes and the surface energy budget equation. It is found that the Penman–Monteith algorithm can also be used to calculate the evaporation ( $E$ ) over ocean with the RH and  $r_s$  values over ocean.

We show that the rate of percentage increase in  $P$  averaged over land is  $\sim 1.65\%/^{\circ}\text{C}$  rise in ocean mean surface air temperature, while the increase in PET is 5.3%/°C, leading to a decrease in  $P$ /PET (i.e., a drier terrestrial climate) by  $\sim 3.4\%/^{\circ}\text{C}$ . Noting similar percentage increase rates for  $P$  over land and evaporation over ocean, we propose a framework for examining the percentage change rates in  $P$ /PET by comparing the change in PET over land with  $E$  over ocean, both estimated using the Penman–Monteith formula. We document the changes in  $T_a$ , RH,  $u$ , and  $R_n - G$  over both land and ocean and quantify their effects on the change in  $P$ /PET. It is found that the contributions from  $T_a$ , RH,  $u$ , and  $R_n - G$  changes to the changes in  $P$ /PET are 53%, 37%, 1%, and 8%, respectively. These contributions are not only determined by the contrasting changes over land and ocean in the relevant surface meteorological variables but also are affected by the

coefficients and background conditions used, which determine the sensitivity of PET ( $E$ ) to the changes in surface variables.

We further separate the effects of the contrasting changes over land versus ocean in the surface meteorological variables and those due to differing responses of PET over land and  $E$  over ocean for given atmospheric changes. A drier terrestrial climate can then be interpreted by (i) enhanced land warming relative to ocean, (ii) a decrease in RH over land but an increase over ocean, (iii) part of increase in net downward radiation going into the deep ocean, and (iv) differing responses of PET over land and  $E$  over ocean to given changes in atmospheric conditions (largely associated with changes in temperatures). The relative contributions to the change in terrestrial mean aridity from these four factors are about 35%, 35%, 15%, and 15%, respectively.

### Appendix A: Change in PET and Contributions From Changes in $T_a$ , RH, $u$ , and $R_n - G$

Here we define  $E = R_n - G$  and use the subscripts “0” and “1” to represent the mean values for the years 1–10 and 61–70 of the simulations, respectively. We also denote the change of a variable  $x$  as  $\delta x = x_1 - x_0$ . The change in PET using equation(1) can then be written in the form

$$\begin{aligned} \delta \text{PET} &= \frac{E_1 \Delta(T_{a1}) + \rho_a c_p e^*(T_{a1})(1 - \text{RH}_1) C_H |u_1|}{\Delta(T_{a1}) + \gamma(1 + r_s C_H |u_1|)} / L_v \\ &\quad - \frac{E_0 \Delta(T_{a0}) + \rho_a c_p e^*(T_{a0})(1 - \text{RH}_0) C_H |u_0|}{\Delta(T_{a0}) + \gamma(1 + r_s C_H |u_0|)} / L_v \\ &= \frac{E_0 \Delta(T_{a1}) + \rho_a c_p e^*(T_{a1})(1 - \text{RH}_0) C_H |u_1|}{\Delta(T_{a1}) + \gamma(1 + r_s C_H |u_1|)} / L_v \\ &\quad - \frac{E_0 \Delta(T_{a0}) + \rho_a c_p e^*(T_{a0})(1 - \text{RH}_0) C_H |u_0|}{\Delta(T_{a0}) + \gamma(1 + r_s C_H |u_0|)} / L_v \\ &\quad + \frac{\delta E \Delta(T_{a1})}{\Delta(T_{a1}) + \gamma(1 + r_s C_H |u_1|)} / L_v \\ &\quad + \frac{\rho_a c_p e^*(T_{a1})(-\delta \text{RH}) C_H |u_1|}{\Delta(T_{a1}) + \gamma(1 + r_s C_H |u_1|)} / L_v \end{aligned}$$

From the above equation and noting that the change in wind speed is small, we can isolate the effect of temperature change by computing the PET using  $T$  in the last 10 years but RH,  $u$ , and  $E$  from the first 10 years minus the PET using the inputs from the first 10 years. The effects of the changes in RH or  $E$  however are estimated by using PET with the inputs from the last 10 years minus that calculated using RH or  $E$  in the first 10 years but other inputs from the last 10 years. The effect of wind speed is estimated similarly to that for the temperature.

#### Acknowledgments

We thank J. Scheff, S. Sherwood, D. Frierson, and J.M. Wallace for their useful discussions. We also thank Ruby Leung, the Editor, and three anonymous reviewers for their constructive comments and suggestions. This study is in part supported by the National Basic Research Program of China (2012CB955303), NSFC grant 41275070, and the NSF grant AGS-1439964. Part of the work was done when Q.F. visited the MPI for Meteorology at Hamburg, with the Humboldt Research Award.

#### References

- Allen, M. R., and W. J. Ingram (2002), Constraints on future changes in climate and the hydrologic cycle, *Nature*, 419(6903), 224–232, doi:10.1038/nature01092.
- Allen, R. G., L. S. Pereira, D. Raes, and M. Smith (1998), Crop evapotranspiration: Guidelines for computing crop water requirements, *FAO Irrigation and Drainage Pap. 56*, Stylus, Sterling, Va.
- Arya, S. P. (2001), *Introduction to Micrometeorology*, Academic Press, San Diego, Calif.
- Bichet, A. M., M. Wild, D. Folini, and C. Schar (2012), Causes for decadal variations of wind speed over land: Sensitivity studies with a global climate model, *Geophys. Res. Lett.*, 39, L11701, doi:10.1029/2012GL01685.
- Burke, E. J., S. J. Brown, and N. Christidis (2006), Modeling the recent evolution of global drought and projections for the twenty-first century with the Hadley Centre climate model, *J. Hydrometeorol.*, 7, 1113–1125.
- Byrne, M. P., and P. A. O’Gorman (2013), Land-ocean warming contrast over a wide range of climates: Convective quasi-equilibrium theory and idealized simulations, *J. Clim.*, 26, 4000–4016.
- Cook, B. I., J. E. Smerdon, R. Seager, and S. Coats (2014), Global warming and 21st century drying, *Clim. Dyn.*, doi:10.1007/s00382-014-2075-y.
- Dai, A. (2013), Increasing drought under global warming in observations and models, *Nat. Clim. Change*, 3, 52–58.
- Dai, A. G. (2011), Characteristics and trends in various forms of the Palmer drought severity index during 1900–2008, *J. Geophys. Res.*, 116, D12115, doi:10.1029/2010JD015541.
- Donohue, R. J., T. R. McVicar, and M. L. Roderick (2010), Assessing the ability of potential evaporation formulations to capture the dynamics in evaporative demand within a changing climate, *J. Hydrol.*, 386, 186–197.
- Feng, S., and Q. Fu (2013), Expansion of global drylands in a warming world, *Atmos. Chem. Phys.*, 13, 10,081–10,094.
- Fu, C. B. (2008), Aridity trend in Northern China, in *Regional Climate Studies of China*, chap. 5, edited by C. B. Fu et al., pp. 155–217, Springer, Berlin.
- Fu, C. B., and Z. G. Ma (2008), Global change and regional aridity trend, *Chin. J. Atmos. Sci.*, 32(4), 752–760.

- Hansen, J., et al. (2005), Earth's energy imbalance: Confirmation and implications, *Science*, 308, 1431–1435.
- Hargreaves, G. H., and Z. A. Samani (1985), Reference crop evapotranspiration from temperature, *Appl. Eng. Agri.*, 1(2), 96–99.
- Held, I. M., and B. J. Soden (2006), Robust responses of the hydrological cycle to global warming, *J. Clim.*, 19, 5686–5699.
- Hulme, M. (1996), Recent climatic change in the world's drylands, *Geophys. Res. Lett.*, 23, 61–64, doi:10.1029/95GL03586.
- Intergovernmental Panel on Climate Change (IPCC) (2013), The physical science basis, in *Contribution of Working Group I to the Fifth Assessment Report of the Intergovernmental Panel on Climate Change*, Cambridge Univ. Press, Cambridge, U. K., and New York.
- Johnson, G. C., et al. (2011), Ocean heat content, *Bull. Am. Meteorol. Soc.*, 92, S81–S84.
- Joshi, M. M., J. M. Gregory, M. J. Webb, D. M. H. Sexton, and T. C. Johns (2008), Mechanisms for the land/sea warming contrast exhibited by simulations of climate change, *Clim. Dyn.*, 30, 455–465.
- Lambert, F. H., and M. J. Webb (2008), Dependency of global mean precipitation on surface temperature, *Geophys. Res. Lett.*, 35, L16706, doi:10.1029/2008GL034838.
- Loeb, N., et al. (2012), Heating of Earth's climate system continues despite lack of surface warming in past decade, *Nat. Geosci.*, 5, 110–113.
- Maidment, D. R. (1993), *Handbook of Hydrology*, McGraw-Hill, New York.
- Manabe, S., M. J. Spelman, and R. J. Stouffer (1992), Transient responses of a coupled ocean-atmosphere model to gradual changes of atmospheric CO<sub>2</sub>. Part II: Seasonal response, *J. Clim.*, 5, 105–126.
- McVicar, T. R., et al. (2012), Global review and synthesis of trends in observed terrestrial near-surface wind speeds: Implications for evaporation, *J. Hydro.*, 416–417, 182–205.
- Middleton, N. J., and D. S. G. Thomas (1992), *UNEP: World Atlas of Desertification*, Edward Arnold, Sevenoaks.
- Mitchell, J. F. B., C. A. Wilson, and W. M. Cunningham (1987), On CO<sub>2</sub> climate sensitivity and model dependence of results, *Q. J. R. Meteorol. Soc.*, 113(475), 293–322, doi:10.1002/qj.49711347517.
- Mortimore, M. (2009), *Dryland Opportunities*, IUCN, Gland, Switzerland, HED, London, U. K., and UNDP, New York.
- O'Gorman, P. A., and C. J. Muller (2010), How closely do changes in surface and column water vapor follow Clausius–Clapeyron scaling in climate change simulations?, *Env. Res. Lett.*, 5, 025207.
- Overpeck, J., and B. Udall (2010), Dry times ahead, *Science*, 328, 1642–1643.
- Padmakumari, B., A. K. Jaswal, and B. N. Goswami (2013), Decrease in evaporation over the Indian monsoon region: Implication on regional hydrological cycle, *Clim. Change*, doi:10.1007/s10584-013-0957-3.
- Pendergrass, A. G., and D. L. Hartmann (2014), The atmospheric energy constraint on global-mean precipitation change, *J. Clim.*, 27, 757–768.
- Reynolds, J. F., et al. (2007), Global desertification: Building a science for dryland development, *Science*, 316, 847–851.
- Richter, I., and S.-P. Xie (2008), Muted precipitation increase in global warming simulations: A surface evaporation perspective, *J. Geophys. Res.*, 113, D24118, doi:10.1029/2008JD010561.
- Rowell, D. P., and R. G. Jones (2006), Causes and uncertainty of future summer drying over Europe, *Clim. Dyn.*, 27, 281–299.
- Scheff, J., and D. Frierson (2014), Scaling potential evapotranspiration with greenhouse warming, *J. Clim.*, 27, 1539–1558.
- Sheffield, J., E. F. Wood, and M. L. Roderick (2012), Little change in global drought over the past 60 yr, *Nature*, 491, 435–438.
- Sherwood, S., and Q. Fu (2014), A drier future?, *Science*, 343, 737–739.
- Simmons, A. J., K. M. Willett, P. D. Jones, P. W. Thorne, and D. P. Dee (2010), Low-frequency variations in surface atmospheric humidity, temperature, and precipitation: Inferences from reanalyses and monthly gridded observational data sets, *J. Geophys. Res.*, 115, D01110, doi:10.1029/2009JD012442.
- Stephens, G. L., and T. D. Ellis (2008), Controls of global-mean precipitation increases in global warming GCM experiments, *J. Clim.*, 21, 6141–6155, doi:10.1175/2008JCLI2144.1.
- Stephens, G. L., et al. (2012), An update on Earth's energy balance in light of the latest global observations, *Nat. Geosci.*, 5, 691–696.
- Taylor, K. E., R. J. Stouffer, and G. A. Meehl (2012), An overview of CMIP5 and the experiment design, *Bull. Am. Meteorol. Soc.*, 93, 485–498.
- United Nations Convention to Combat Desertification (1994), U. N. Doc. A/A C. 241/27, 33 I. L. M. 1328, United Nations.
- Wang, K. C., R. E. Dickinson, and S. Liang (2012), Global atmospheric evaporative demand over land from 1973 to 2008, *J. Clim.*, 25, 8353–8361.
- Wever, N. (2012), Quantifying trends in surface roughness and the effect on surface wind speed observations, *J. Geophys. Res.*, 117, D11104, doi:10.1029/2011JD017118.
- Yang, X., Z. Yao, Z. Q. Li, and T. Fan (2013), Heavy air pollution suppresses summer thunderstorms in central China, *J. Atmos. Solar-Terrestrial Phys.*, 95–96, 28–40.
- Zhang, X., and X. Cai (2013), Climate change impacts on global agricultural water deficit, *Geophys. Res. Lett.*, 40, 1111–1117, doi:10.1002/grl.50279.